 doi:10.20944/preprints202209.0284.v1

Article

Research on Tire Groove Depth Detection System based on MVR

Feng Qian [1], Xingwen Li [1], Neng Zhu [1,*], Mingda Wang [2,*], Jie Wang [1], Xiaowei Xu [1], Beijia Zhang [1], Mengjie Liu [1] and Qinghua Qi [1]

[1] School of Automotive and Transportation Engineering, Wuhan University of Science and Technology;
[2] Chinese Academy of Environmental Sciences;
* Correspondence: NZ:znqc@wust.edu.cn,MW: wangmingda@vecc-mee.org.cn

Abstract: The change of tire groove depth will have a huge impact on tire performance, and the use of excessively worn tires is not conducive to the driving safety of automobiles. Tire groove depth detection has become one of the annual inspection items of automobiles, but the research on its related detection technology is still relatively backward. Based on the principle of monocular vision ranging (MVR), image processing technology and cloud platform technology, this paper develops a tire groove depth detection system, which realizes non-destructive detection of tire groove depth. In addition, the system uses the cloud platform to store the test results, and builds a multi-level data management system, allowing car owners to keep track of the tire wear status and historical changes, which is of great significance to ensuring driving safety.

Keywords: tire groove depth, MVR, cloud platform

1. Introduction

In 2021, the number of civil vehicles in China will reach 301.51 million, and the continuous growth of the number of vehicles will bring increasing safety issues. In the same year, a total of 244,937 road traffic accidents occurred, resulting in 63,194 injuries and 258,532 deaths. The traffic accident rate in China is much higher than that of western developed countries. As one of the main causes of traffic accidents, tire failure has become an important research direction to ensure tire safety.

Tire tread wear can lead to reduced tire performance [1] (braking distance, critical hydroplaning speed, etc.), thereby increasing the risk of vehicle driving. GB38900-2020 "Motor Vehicle Safety Technical Inspection Items and Methods" clearly stipulates that the tire groove depth test item should be added to the annual vehicle inspection. Among them, the depth of the steering wheel crown pattern for motor vehicles should be greater than or equal to 3.2mm, and the depth of non-steering wheels should be greater than or equal to 1.6mm. Obviously, the research of tire groove depth measurement technology has great social significance and economic value.

Non-destructive testing (NDT) is the main development direction of tire inspection technology (TIT). Common tire NDT include: phase-shift shearing speckle interference technology [2], X-ray imaging testing technology [3], ultrasonic testing technology [4], electrical Pulse detection technology [5], electromagnetic wave technology [6], image recognition technology [7,8]. The TIT is mainly based on defect detection (damage, air bubbles, sub-port exit, lack of glue, exposed lines, cracks, etc.) [9], while the development of related technologies for groove depth detection is still relatively backward, and artificial depth gauges are generally used for measurement, which has the defects of low efficiency and great human influence on the measurement results. In this paper, based on the principle of MVR, a method for measuring the depth of tire grooves is designed, and the design of the detection device is completed. Simultaneously, in order to realize the unified management of test results, a data management cloud platform was designed and

Preprints (www.preprints.org) | NOT PEER-REVIEWED | Posted: 20 September 2022 doi:10.20944/preprints202209.0284.v1

developed, and car owners can view the tire wear changes in real time and understand the tire wear changes to ensure tire safety.

2. Groove Measurement Algorithm

2.1. The principle of MVR

The basic principle of MVR is to use a single camera to shoot the target to be measured [10], as to obtain the imaging pixel value of the target, and then calculate the actual size of the target through the imaging ratio of the camera [11]. According to the different acquisition methods, the imaging ratio can be divided into two types: standard reference acquisition (SRA) and camera parameter calibration acquisition (CPCA). The principle of the SRA is shown in Figure 1(a), P_1P_2 is the measured distance, S_1S_2 is a reference object whose actual size is known, and they is located in the same plane parallel to the imaging plane, $P_1'P_2'$ and $S_1'S_2'$ is the respectively their imaging. If it is known that the actual length of $S_1'S_2'$ is l_S, the pixel distance in the coordinate system of $P_1'P_2'$ and $S_1'S_2'$ is l_P' and l_S', the actual distance l_P can be calculated according to the following formula:

$$l_P = \frac{l_P' l_S}{l_S'} \tag{1}$$

If the pixel coordinates of the imaging point are: $S_1'(x_{S1}, y_{S1})$, $S_2'(x_{S2}, y_{S2})$, $P_1'(x_{P1}, y_{P1})$ and $P_2'(x_{P2}, y_{P2})$, then l_P'、l_S' can be calculated as shown in formulas (2)and (3):

$$l_P' = \sqrt{(x_{P1} - x_{P1}')^2 + (y_{P1} - y_{P1}')^2} \tag{2}$$

$$l_S' = \sqrt{(x_{S1} - x_{S1}')^2 + (y_{S1} - y_{S1}')^2} \tag{3}$$

Substitute formulas (2)(3) into formula (1) to get l_P.

$$l_P = \frac{l_S \sqrt{(x_{P1} - x_{P1}')^2 + (y_{P1} - y_{P1}')^2}}{\sqrt{(x_{S1} - x_{S1}')^2 + (y_{S1} - y_{S1}')^2}} \tag{4}$$

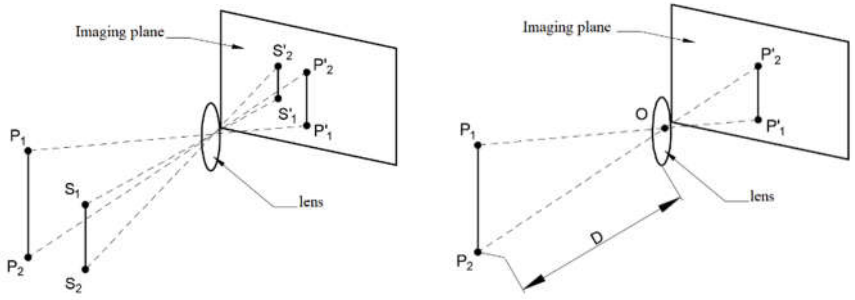

(a) SRA imaging ratio b) CPCA imaging ratio

Figure 1. Two methods of obtaining reference objects.

Figure 1(b) show the principle of obtaining the imaging ratio through the CPCA. The CPCA does not need to set a reference, directly uses the calibration method to get the camera imaging ratio. Only l_P' be measured and the distance D between the object to be measured and the lens can be obtained to get the actual size of the object. It can be seen from Figure 1.b that there is a similar relationship between the triangle OP_1P_2 and the triangle $OP_1'P_2'$,so when the proportional coefficient relationship at different distances D is known, l_P can be obtained through the length l_P' according to the similarity principle.

Preprints (www.preprints.org) | NOT PEER-REVIEWED | Posted: 20 September 2022 doi:10.20944/preprints202209.0284.v1

$$l_P = K l_P^{'} \tag{5}$$

Substitute into formula (2) to get:

$$l_p = K\sqrt{(x_{P1} - x_{P1}^{'})^2 + (y_{P1} - y_{P1}^{'})^2} \tag{6}$$

When using the SRA to obtain the imaging scale, $l_P^{'}$ is prone to deviation. Relatively, the imaging scale obtained by the CPCA is more accurate. For improving the measurement accuracy, there adopts the CPCA to obtain the imaging ratio.

2.2. The principle of MVR

Figure 2 shows a scheme for collecting a tire groove image, which is taken from the tangential direction of the tire outer profile circular surface to obtain. Preprocessing groove images by image processing technology to achieve separation of tire groove features. the profile information is extracted, then the groove depth is calculated based on the principle of MVR.

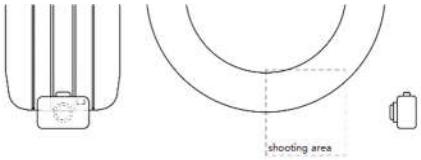

Figure 2. Image acquisition scheme.

When the image features are vague, the complexity of image preprocessing will increase accordingly, and light source compensation is required to enhance the target information during image acquisition. In this paper, a linear laser is used for compensation, and the sipe feature is enlarged by irradiating the sipe area [12]. In addition, the tires are shaded to reduce ambient light interference. The acquired image is shown in Figure 3.

Figure 3. Captured image diagram.

When the background is too large, it will also increase the difficulty of extraction. The region of interests is extracted to reduce the influence of irrelevant background [13]. By adding a marquee to the real-time image of the camera and adjusting the positional relationship between tire and camera. Then the tire pattern is placed in the marquee. After shooting, crop the selected area to reduce the invalid area of the picture. Figure 4 is a cropping effect image taken by a 200W pixel camera.

Figure 4. Cropping effect diagram.

2.3. Image preprocessing

The goal of image preprocessing is to separate groove feature information from images. It is necessary to minimize steps in the processing to prevent distortion caused. First, grayscale the image. Grayscale refers to converting a three-dimensional channels (RGB) color image into a one-dimensional grayscale image. Through grayscale processing, the

Preprints (www.preprints.org) | NOT PEER-REVIEWED | Posted: 20 September 2022 doi:10.20944/preprints202209.0284.v1

amount of image data and the input amount of subsequent deep processing can be reduced, so the processing calculation amount can be simple. The extraction of groove features requires high global changes, and the global mapping method is used for grayscale processing. Figure 5 shows the operation results of several commonly used grayscale algorithms. It can be found that there is no obvious difference between the advantages and disadvantages of each algorithm. Here, the weighted average method is used as the grayscale algorithm.

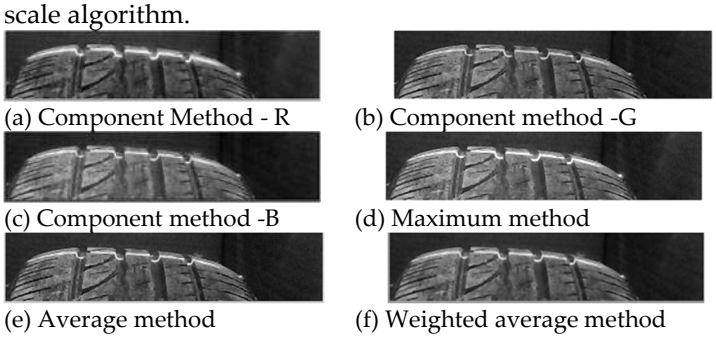

(a) Component Method - R (b) Component method -G

(c) Component method -B (d) Maximum method

(e) Average method (f) Weighted average method

Figure 5. Grayscale effect comparison.

There is an obvious difference between the tire and the invalid background after grayscale, and setting a reasonable threshold for binarization can separate the tire from the background. Thresholds can be divided into simple thresholds (ST) and dynamic thresholds (DT) according to the acquisition methods. The ST is to directly set a fixed value manually as the global threshold. Due to the influence of tire surface color and light, it cannot meet the processing needs of various environments, while the DT can be calculated according to the different images to ensure the applicability of the detection algorithm in different detection environments. Figure 6 shows the binarization results of two commonly used DT (Otsu method and trigonometry). The Otsu method has well-preserved groove details and less noise. The trigonometry basically loses the groove characteristics and has more noise points, so here The Otsu method is used for dynamic threshold calculation.

(a) Otsu's Algorithm Results (b) Trigonometric result

Figure 6. Comparison of binarization results.

2.4. Calculation of groove depth

After preprocessing, the tire is basically separated from the invalid background, and the pixel coordinate system shown in Figure 7 is constructed. The collection of maximum coordinate points constitutes a scatter plot of the tire surface profile, and the results are shown in Figure 8.

Figure 7. Image Coordinate System.

Preprints (www.preprints.org) | NOT PEER-REVIEWED | Posted: 20 September 2022 doi:10.20944/preprints202209.0284.v1

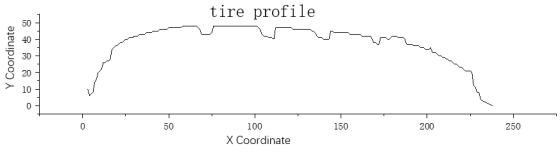

Figure 8. Tire Surface Profile.

Aiming at the extraction of grooves in tire profile, this paper proposes an extraction algorithm based on polynomial fitting method. By fitting the tire surface tangent, combined with the actual pattern change of the tire to calculate the depth of the tire groove. Table 1 and Figure 9 are the comparison of the fitting results of different orders of polynomials. It is found that when the fitting formula reaches the sixth order and the order of the formula is increased, the increase rate of the residual sum of squares and R square is significantly slower than that of the fourth and fifth orders, and the fitting curve no longer changes significantly. Therefore, the sixth-order polynomial as a fitting formula has satisfied needs.

Table 1. Comparison of fitting effects.

Fitting order	Quantity residual sum of squares	R squared
fourth order	1238.84928	0.95055
fifth order	1149.25383	0.95413
sixth order	858.41735	0.96574
seventh order	825.21358	0.96706

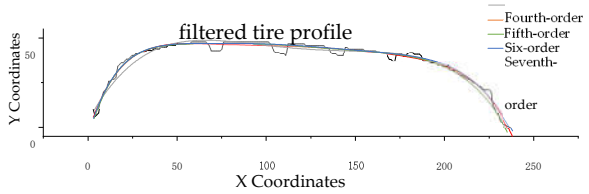

Figure 9. Comparison of fitting results.

Figure 10 shows the calculated difference between the fitted curve and the Y coordinate of the contour point. The groove depth is extracted through some steps, and 4 groove pixel coordinates are obtained. The pixel coordinate depth value is $H^{'}$. When the imaging scale coefficient obtained by calibration is K, the actual distance H is calculated by the following formula:

$$H = H^{'}K \tag{7}$$

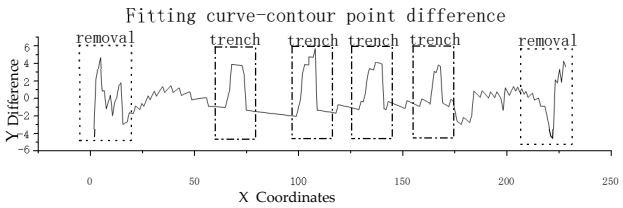

Figure 10. The difference between the fitted curve and the contour point.

3. Detection device

The detection device consists of a detection stand and detection software. Based on the above groove measurement algorithm image acquisition scheme, the structure of the equipment is designed, and the matching software is developed.

Preprints (www.preprints.org) | NOT PEER-REVIEWED | Posted: 20 September 2022 doi:10.20944/preprints202209.0284.v1

3.1. Test stand

Through the analysis of the image acquisition scheme of the groove measurement algorithm, the detection bench as shown in Figure 11 is designed. In addition to the lasers and depth cameras required for depth measurement, three defect detection cameras are added, and inspectors can manually detect tire surface defects through the cameras.

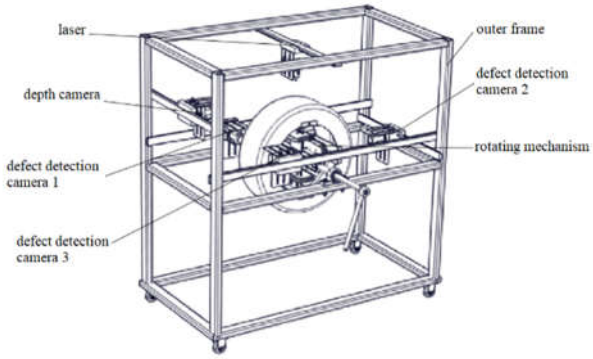

Figure 11. Test stand.

3.2. Detection software

The main functions of the inspection software include the collection and processing of the tire image information of the inspection device, the display of the inspection results, and the transmission of the inspection results to the data management platform. Table 2 lists the main functions of the interface.

Table 2. Detection software interface and functional composition.

Interface composition	Function introduction
Login interface	User login
Detection interface	Mode options, camera preview, vehicle data query, data upload, log view, test result display

Figure 12 shows the detection software architecture, which is divided into two parts: the interaction layer and the data processing layer. The interaction layer is the software interaction interface, which mainly realizes event triggering, information display, etc., including two interfaces of login and detection. The data processing layer includes network communication module, video module and detection module.

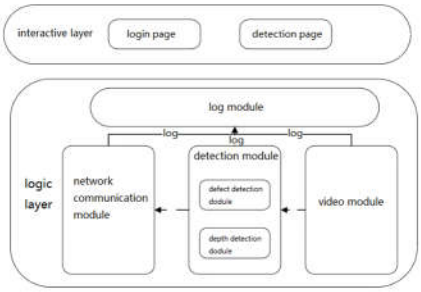

Figure 12. Detection software framework.

The detection software is written in python. Figure 13 is the effect diagram of the detection software detection interface. Including detection vehicle query window, detection mode selection, access camera and tire detection result display, etc.

Preprints (www.preprints.org) | NOT PEER-REVIEWED | Posted: 20 September 2022 doi:10.20944/preprints202209.0284.v1

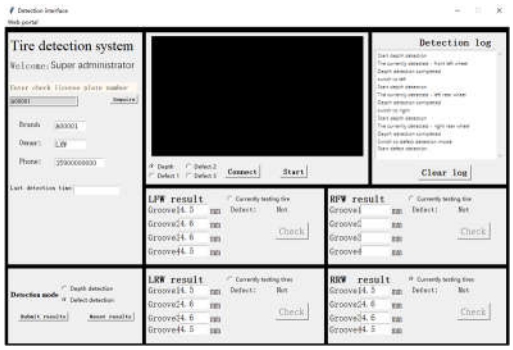

Figure 13. Detection interface.

3.3. Device testing

The error tire profile extraction of groove measurement method is related to groove calculation. Table 3 shows the measurement results of new and ageing tires using the testing device. Taking the measurement results of the electronic depth gauge as a reference. In the comparison of the testing results, the average error of the new tire is 0.16mm, and the difference between the maximum error and the minimum error is 0.07mm. The average error of used tires is 0.16mm, and the difference between the maximum error and the minimum error is 0.07mm. The maximum error of the 8 measurement results is 0.2mm.

Table 3. Comparison of measurement results

Tires (unit: mm)		Depth Gauges Measurement	photogrammetry Quantitative method	Relative deviation
New tireT125/80R18	groove 1	7.61	7.74	0.13
	groove 2	7.74	7.89	0.15
	groove 3	7.69	7.89	0.20
	groove 4	7.62	7.78	0.16
old tire 245/45R18	groove 1	5.07	5.26	0.19
	groove 2	5.43	5.60	0.17
	groove 3	5.54	5.66	0.12
	groove 4	5.02	5.18	0.16

4. Data Management Cloud Platform

4.1. Functional Analysis

The management platform is developed with a front-end and back-end separation structure, mainly for cloud storage and management of tire test results, realizing the monitoring of groove wear changes in the tire life cycle.Figure 14 shows the functional structure, which is mainly divided into three parts.

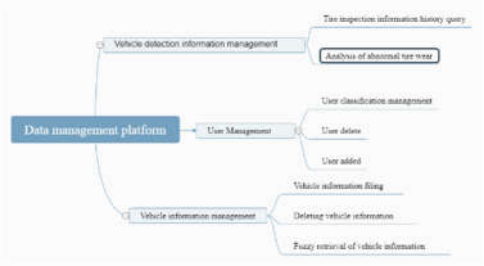

Figure 14. Functional composition of the platform.

Vehicle inspection information management can perform historical inquiry on vehicle inspection information, so that inspectors and car owners have a comprehensive understanding of vehicle tire wear changes, and can simply analyze abnormal tire wear.

Preprints (www.preprints.org) | NOT PEER-REVIEWED | Posted: 20 September 2022 doi:10.20944/preprints202209.0284.v1

Table 4 shows the common abnormal wear and causes of tire grooves. When abnormal wear occurs, the platform will remind the possible causes accordingly.

Table 4. Common abnormal wear and cause analysis of tire grooves.

wear phenomenon	possible reason
The middle groove is severely worn	tire pressure too high
Severely worn grooves on both sides	Low tire pressure, prolonged overweight
Severe wear on one side groove	Incorrect targeting parameters
Serious wear on a single tire	The function of the suspension system is reduced, the supporting parts are bent and deformed, and the dynamic and static balance problems

User management consists of three types of users: super administrator, store and inspection personnel, which can classify and manage inspection vehicles according to different users. The vehicle information management adopts the vehicle filing mechanism, and through the advance filing of basic vehicle information, a data management system with a single vehicle as the smallest unit is constructed.

4.2. Functional Analysis

The platform is developed based on Vue (front-end framework), springboot (back-end framework), and mysql database. Figure 15 is a partial platform implementation renderings.

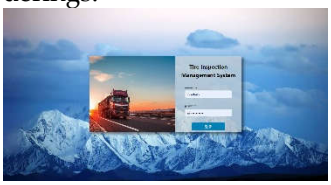

(a) Login interface

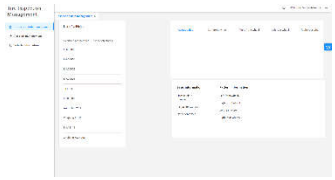

(b) Inspection data interface

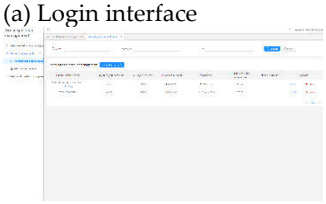

(c)Manufacturer account management

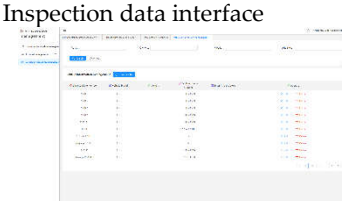

(d) Vehicle information management

Figure 15. Functional composition of the platform.

5. Conclusion

Based on the principle of MVR and image processing technology, this paper realizes the measurement of the depth of the tire groove by taking pictures of the tire groove at a specific angle. According to the measurement algorithm, the structure design of the testing bench is carried out, and the matching testing software is developed. In order to realize the unified management of detection data, a data management cloud platform is built based on cloud platform technology. This paper has completed the research of tire groove depth measurement algorithm, the design and development of detection device and related software, which is of great significance to ensure tire safety and reduce traffic accidents.

References

1. Leo E, Pezzola M E, Pagliara C, et al. Effects of tire wear on motorcycle dynamic[C]. Symposium on the Dynamics and Control of Single Track Vehicles, 2020.
2. Vishnyakov G N, Ivanov A D, Levin G G, et al. Phase-shift speckle-shearing interferometry[J]. Quantum Electronics, 2020, 50(7): 636.
3. Sedaghat Y, Parhizgar N, Keshavarz A. Automatic defects detection using neighborhood windows features in tire X-ray images[J]. International Journal of Nonlinear Analysis and Applications, 2021, 12(Special Issue): 2493-2508.

4. Yung W H, Yung L C, Hua L H. A study of the durability properties of waste tire rubber applied to self-compacting concrete[J]. Construction and Building Materials, 2013, 41: 665-672.
5. Zheng Z, Zhang S, Yu B, et al. Defect inspection in tire radiographic image using concise semantic segmentation[J]. IEEE Access, 2020, 8: 112674-112687.
6. Wang F, Zhu H, Li Y, et al. Microwave heating mechanism and Self-healing performance of scrap tire pyrolysis carbon black modified bitumen[J]. Construction and Building Materials, 2022, 341: 127873.
7. Zhu J, Han K, Wang S. Automobile tire life prediction based on image processing and machine learning technology[J]. Advances in Mechanical Engineering, 2021, 13(3): 16878140211002727.
8. Zhang S, Wu Y, Chang J. Tire damage image recognition based on improved convolutional neural network[C]//2020 IEEE International Conference on Information Technology, Big Data and Artificial Intelligence (ICIBA). IEEE, 2020, 1: 1433-1437.
9. Chen J, Li Y, Zhao J. X-ray of tire defects detection via modified faster R-CNN[C]//2019 2nd International Conference on Safety Produce Informatization (IICSPI). IEEE, 2019: 257-260.
10. Zhang L, Feng S, Shan H, et al. Tractor-trailer-train braking time sequence detection based on monocular vision[J]. Advances in Mechanical Engineering, 2021, 13(12): 16878140211067045.
11. Sanz-Ablanedo E, Chandler J H, Rodríguez-Pérez J R, et al. Accuracy of unmanned aerial vehicle (UAV) and SfM photogrammetry survey as a function of the number and location of ground control points used[J]. Remote Sensing, 2018, 10(10): 1606.
12. Yang H, Jiang Y, Deng F, et al. Detection of Bubble Defects on Tire Surface Based on Line Laser and Machine Vision[J]. Processes, 2022, 10(2): 255.
13. Aggarwal A, Rani A, Kumar M. A robust method to authenticate car license plates using segmentation and ROI based approach[J]. Smart and Sustainable Built Environment, 2019.